A component model for column face in bending of extended HolloBolt connections

Mohammed Mahmood [1] and Walid Tizani [2]

[1] Department of Civil Engineering, University of Diyala, Iraq

[2] Department of Civil Engineering, University of Nottingham, UK

Abstract

Extended HolloBolt (EHB) is a practical anchored blind bolting system for concrete-filled steel sections. One of the failure modes of EHB connections is the bending of the column face component. Up to date, no analytical model to estimate the strength and stiffness of this component have been proposed. This paper aims to develop such model to capture the principal aspects of the overall behaviour of the component, such as its strength and stiffness at different key stages, to represent the component behaviour. The component strength is assumed to be provided by the steel hollow section plate bending and the anchored action. The steel hollow section plate strength models were developed based on the yield line theory. The anchored strength was considered equivalent to the load required to initiate a concrete cone failure. The component stiffness models were formulated using elastic springs, one at each bolt location. The component stiffness was taken equal to the summation of springs stiffness as they act in parallel. The overall bending behaviour of the component was represented by a quad-linear model. The stiffness of the post yield parts of the model was considered as a percentage of the initial stiffness of the component. The model was validated with the available data in the literature and they provided reliable results, which can be considered as a benchmark for the design of EHB connections. This model can be later extended and generalized for other similar blind bolts connections.

Keywords: *Anchored bolted connections, Column face bending, Extended HolloBolt connections, Concrete filled tubular columns, Component model, Strength and stiffness model.*

1. Introduction

The Extended HolloBolt (EHB) is a practical anchored blind bolting system for concrete-filled Steel Hollow Sections (SHS). Its tensile performance was investigated and it showed similar behaviour to the standard bolts in terms of strength and failure mode [1, 2]. The bending of the column face component is one of the failure modes in EHB connections. However, there are no existing models to estimate the strength and stiffness of this component. A considerable amount of literature has been published on developing analytical models for the bending behaviour of the column face component with different connecting methods such as using blind bolts or welding some fitting to the column face. Some of these studies proposed models for connections to concrete-filled structural hollow sections and others for unfilled. Ghobarah et al. [3] developed an analytical model for the initial stiffness of high strength blind bolts connections. The column face component was modelled as a thin plate with a span length equal to the clear distance between the internal sides of the column walls. In the transverse direction, the column face was assumed to have an infinite width since there was no restrain near the connection. In the direction normal to the column face, it was modelled as a fixed ends plate because the concrete infill prevents the column wall deformation. The post-elastic stiffness of the connection was considered as a percentage from the initial stiffness and it was taken as 7% of the initial stiffness. The approach of Ghobarah et al. [3] was successfully adopted in many studies to estimate the stiffness of the column face component for different types of blind bolt connections. In 2009, Wang et al. [4] tested full-scale HolloBolt (HB) connections to circular and square concrete filled hollow sections. The deflection coefficient in Ghobarah et al. [3] model was modified to calculate the initial bending stiffness of the column face component. In another study, Lee et al. [5] suggested a reduction factor for predicting the initial bending stiffness of the column face for blind bolted connections to unfilled SHS using the Ajax ONESIDE bolt. The reduction factor was added to consider the flexibility of the column walls in the case of unfilled SHS.

Jaspart [6], used a fan yield line mechanism for a single row of bolts in minor axis connection for a single bolt row in tension and derived the formula for the component plastic resistance. The same

formula was adopted by Silva et al. [7] to calculate the plastic resistance for welded studs connection to concrete filled hollow sections. Harada et al. [8], stated that the weld connection of structural hollow sections and wide flange beams can fail by welding fracture especially under seismic loads. Therefore, they suggested the replacement of the weld connection by a T-stub bolted, using high strength bolts. The yield load and the collapse load of the column face were calculated based on the yield line theory.

An equivalent rigid strip model for estimating the bending stiffness for the column web in minor axis connections for open sections was developed by Neves and Gomes [9]. Silva et al. [10] applied this model to calculate the bending stiffness for the column face of concrete-filled hollow sections (Figure 1). The model assumes that the column face is loaded by a rigid area. The width of the rigid area is controlled by the bolt head/nut size and its length controlled by the gauge distance in addition to the bolt head/nut size. The column face was represented as a plate with fixed supports at the SHS wall centrelines and free at the remaining two edges.
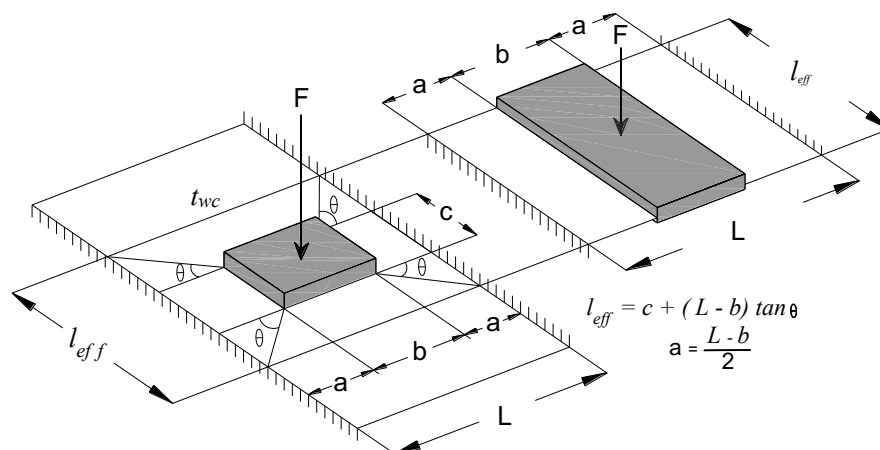

Figure 1: Rigid strip model for column face component of concrete-filled hollow section [10]

Elghazouli et al. [11] investigated the monotonic and cyclic behaviour of HB connections to unfilled SHS. The column face component was assumed to be acting in series with the HB. A modified version of the stiffness model for open sections was proposed for estimating the initial stiffness of the column face and the post yield stiffness was assumed to be 10% of the initial stiffness. The same approach was successfully adopted by Málaga-Chuquitaype and Elghazouli [12] and [13] and Liu et al. [14] and [15].

To find the plastic resistance of the column face component in Ajax ONESIDE connections, Lee et al. [5] used two formulas. The first was CIDECT Design Guide9 formula [16] and the second was proposed by Mourad [17]. Both of these formulas were developed based on the yield line theory. It was stated that reasonable results were obtained from both of them; however, Mourad's formula was closer to the finite element prediction.

Park and Wang [18], derived an analytical model to predict the initial stiffness of blind bolted end plate connections to unfilled structural hollow sections based on Timoshenko plate theory and the work that was performed by Jaspart et al. [19] and Weynand et al. [20]. The study neglected the interaction between the bolt rows and assumed that each bolt row can act individually so that each row can be represented as a joint component. Thai and Uy [21] presented a component-based model to predict the load-deformation response of axially-loaded through-diaphragm connections to concrete-filled SHS columns. The model considered the contributions from the column tube face in bending based on the yield line method. Two simplified analytical models were proposed by Wang et al. [22] to calculate the initial stiffness of HB connections to double-skin tubular columns. The same approach was employed by Wang et al. [23] to predict the initial stiffness of blind bolts connections to the concrete-encased concrete-filled steel tube.

The component method for different types of steel connections is well detailed in EC3 [24]. It represents a practical approach for analysing the connections by simplifying the connection into a series of individual components. For EHB connections, the component models have not yet been developed. Several studies proposed analytical models for the strength and stiffness of blind bolted connections. These models cannot be applied to the EHB due to the significant

difference in the bolt geometry and the contact interactions arising from anchoring the bolts inside the concrete. Therefore, there is a need for analytical models for the strength and stiffness of the different components of the EHB connections.   This paper devises component model for the bending behaviour of the column face component in EHB connections. The model can be considered as a significant step towards the development of design guidance for this connection based on the component method. The availability of such guidance in codes of practice will widen the use of the SHS in structural applications.

2. Modelling of the Column Face Component

To simulate the behaviour of the column face component in the tension side of EHB connections, the face of the SHS is separated from the rest of the section and considered as a long plate. This plate is supported at its longitudinal edges (along the length of the SHS) by the SHS walls. The concrete infill provides support to the SHS walls and prevents rotation along the longitudinal edges of the column face. Thus, the SHS walls act as fixed supports for the column face [3, 7, 17]. The transverse edges of the component were assumed free as long as there are no restraints along the column length close to the connection. Accordingly, a column face component connected by four bolts in tension is modelled as a long plate fixed along the longitudinal edges and free along the transverse edges. The applied load is assumed to be equally distributed between the bolts. Therefore, the column face plate is assumed to be subjected to four equal forces at the locations of the bolts (Figure 2). The contribution of the concrete infill in resisting the applied load is considered as an additional thickness to the column face plate [25].
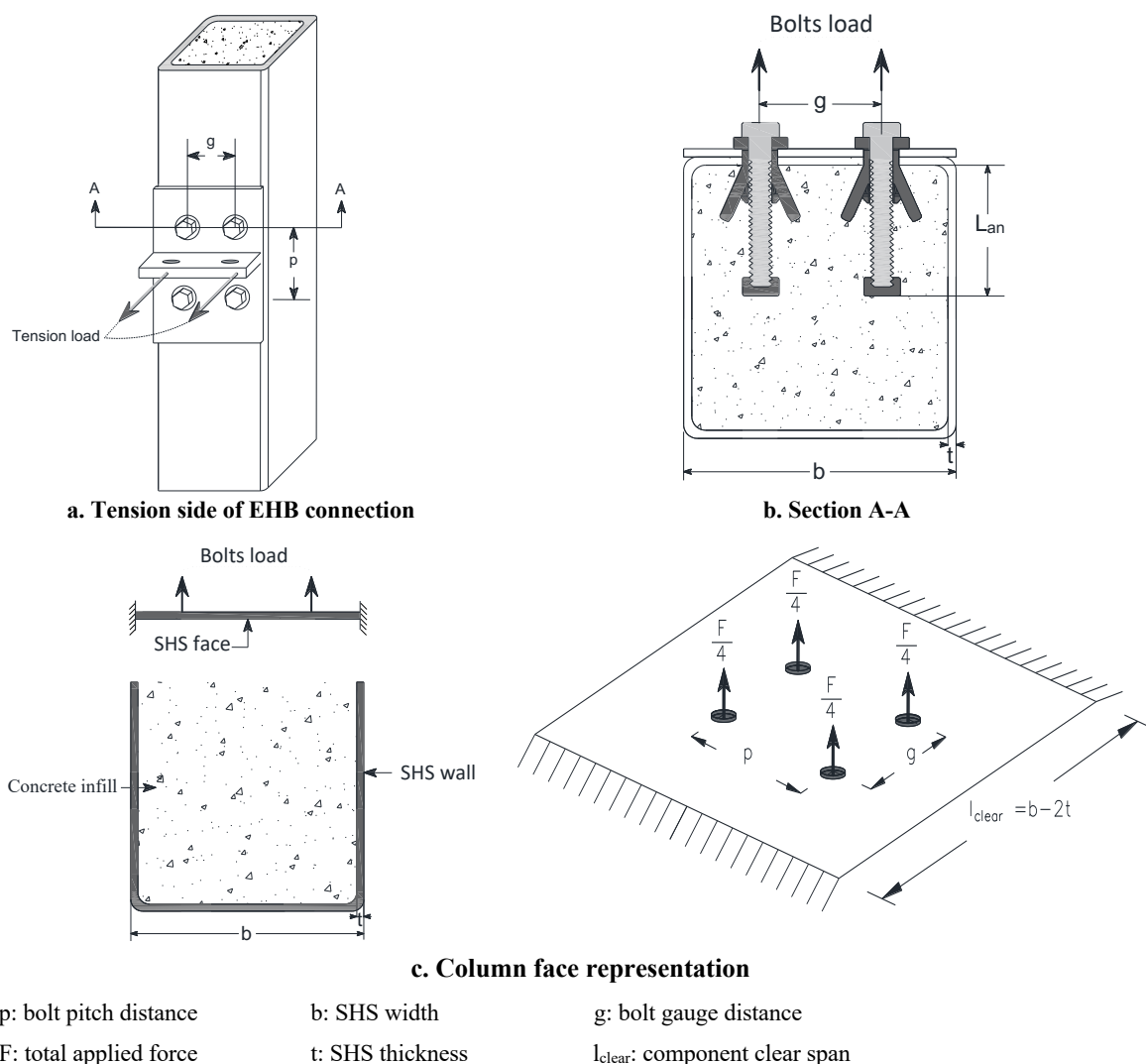
a. Tension side of EHB connection

b. Section A-A

c. Column face representation

p: bolt pitch distance   b: SHS width   g: bolt gauge distance

F: total applied force   t: SHS thickness l_{clear}: component clear span

Figure 2: Modelling of the column face component

3

3. Column Face Bending Strength

The development of the EHB is based on anchoring part of it inside the concrete to involve the concrete in the resistance of the applied load. The failure mechanism of the EHB connection was presented in details in Tizani et al. [26]. It was confirmed that, at the ultimate limit state the failure mode is EHB anchorage failure followed by yielding of the column face plate (Figure 3). Thus, the strength of the column face component is equal to the sum of the SHS plate strength and the anchorage resistance. The strength of column flange, face and web when they act as connection faces was successfully estimated using yield line theory [27, 28]. The Eurocode also adopted the yield line theory in the design of steel joints [24]. In this study, the yield line theory was used to develop analytical model for the plastic strength of the SHS plate. The developed model quantifies the contribution of the SHS plate to the overall resistance of the component. The contribution of the anchored bolts in the component plastic resistance was quantified by considering the work required to initiate a concrete cone failure. A geometry coefficient (γ_1), which was proposed by Mahmood [29] to consider the effect of the column face width and the bolt anchored length on component strength was adopted in this study.
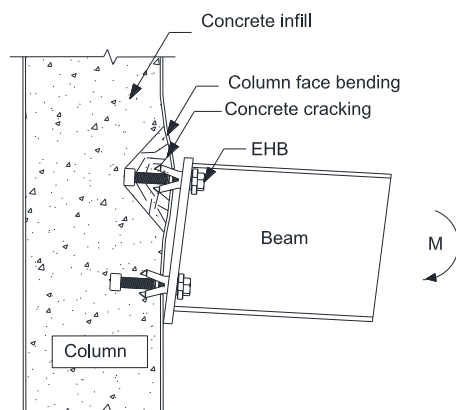

Figure 3: Column face bending failure

The component plastic resistance is

$$F_p = (F_{ps} + F_{pa}) \times \gamma_1 \tag{1}$$

where

F_p: column face component plastic resistance

F_{ps}: SHS plate plastic resistance

F_{pa}: anchorage plastic resistance

$\gamma_1 = \frac{1.1 \, L_{an} + 130}{b}$

L_{an}: EHB anchored length

3.1. SHS plate plastic resistance

Six possible modes of yield line patterns were assumed for the SHS plate (Figure 4) to estimate its plastic capacity and find the dominant mode. The yield lines were assumed to extend to cover the corners of the tubular section [26]. The yield lines patterns vary based on the bolt pitch (p) and gauge (g) distances. For example, Mode 1 exists in the case of large p and g and Mode 2 occurs with small g and large p. Mode 3 and Mode 6 are the simplified modes for Mode 2 and Mode 5 respectively. The principle of virtual work was applied to develop the SHS plate plastic resistance formulas for each mode in Figure 4. The plastic resistance of the SHS plate for each mode is obtained by equating the external and internal works.
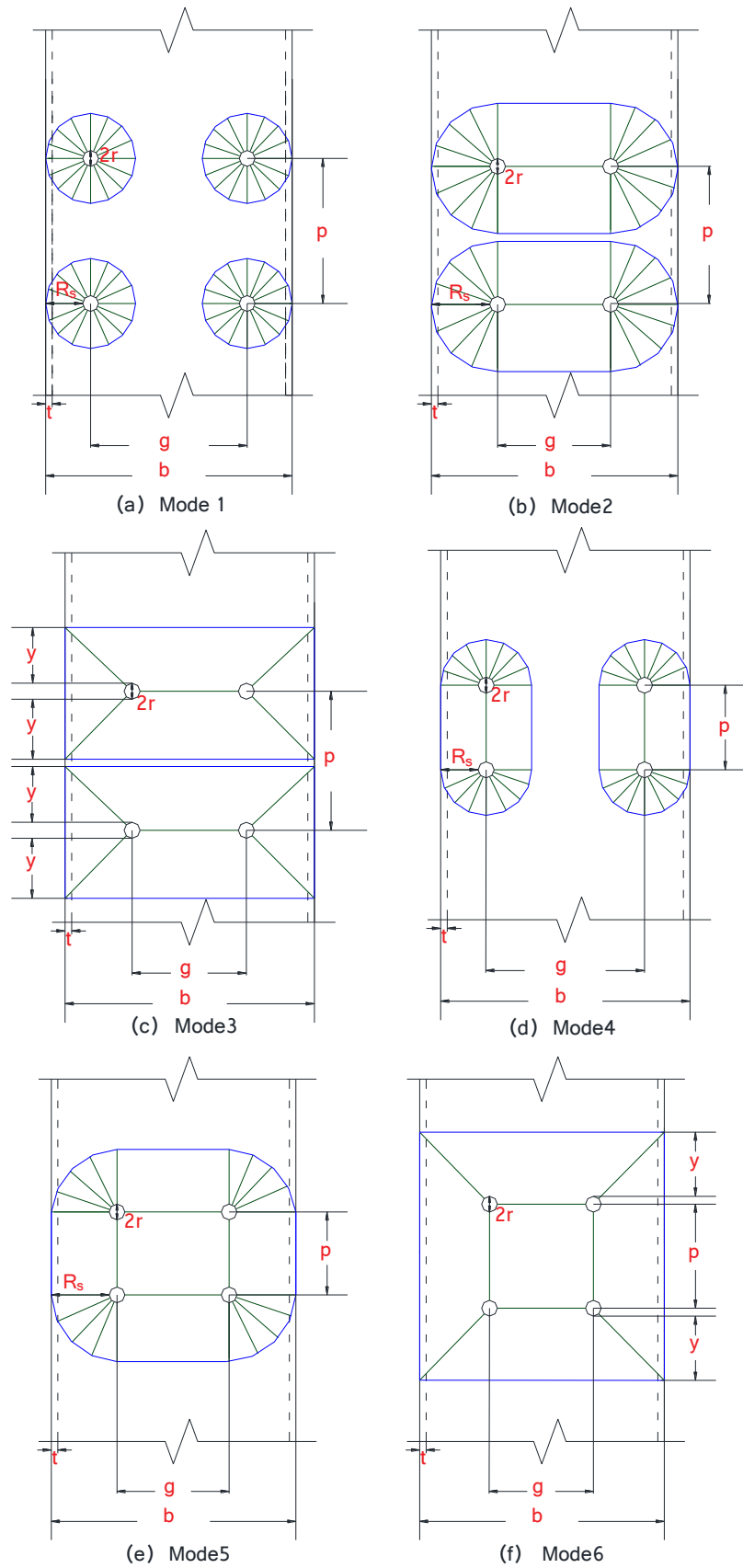
4

Figure 4: Theoretical yield line patterns of square hollow section loaded at four points

- **Mode 1**

The yielded area in this mode consists of four circles (Figure 4, a). Equation (2) represents the plastic resistance of the SHS plate.

$$F_{ps\,1} = 8\pi M_p \times \left(1 + \frac{R_s + r}{R_s}\right)$$ (2)

where

M_p: the plastic moment of resistance for a unit length of the SHS plate $= \frac{f_y \times t^2}{4}$

f_y : yield strength of SHS plate

t : the thickness of the SHS plate

R_s: radius of the yielded area $= \frac{b - g - 2r}{2}$

b: width of the SHS

g: bolt gauge distance

r: radius of the bolt hole

- **Mode 2**

Figure 4, b shows that for each row there are two halves of fan yielding and three connecting yield lines. Therefore, the plastic resistance for Mode 2 is calculated by considering the work required to generate two fans patterns plus the connecting yield lines. Equation (3) characterises the plastic resistance of the SHS plate for Mode 2.

$$F_{ps\,2\,d} = 4\pi M_p \times \left(1 + \frac{R_s + r}{R_s}\right) + 4M_p \times \left(\frac{2g - 2r}{R_s + r}\right)$$ (3)

For a component with only one row of tow EHBs in tension, equation (4) can be used to calculate the plastic resistance of the SHS plate.

$$F_{ps\,2\,s} = 2\pi M_p \times \left(1 + \frac{R_s + r}{R_s}\right) + 2M_p \times \left(\frac{2g - 2r}{R_s + r}\right)$$ (4)

- **Mode 3**

In this mode, there is no fan yielding mechanism. It is a simplified version of Mode 2. Equation (5) was derived to calculate the plastic resistance of the SHS with the yield patterns according to Mode 3.

$$F_{ps\,3} = 8M_p \times \left(\frac{g + 2R_s + r}{y + r} + \frac{2y + r}{R_s}\right)$$ (5)

To find the maximum value of the unknown dimension y, the first derivative of equation (5) with respect to y was equated to zero.

$$y = \sqrt{\frac{R_s\,(g + 2R_s + r)}{2}}$$ (6)

In the case of only one row of two EHBs in tension, equation (7) can be used to calculate the plastic resistance for the SHS plate.

$$F_{ps\,3} = 4M_p \times \left(\frac{g + 2R_s + r}{y + r} + \frac{2y + r}{R_s}\right)$$ (7)

- **Mode 4**

The yield patterns for Mode 4 are similar to Mode 2. However, the connecting lines here extend along with the bolt pitch distance, whereas in Mode 2 they are with the bolt gauge distance (Figure 4, d). The plastic resistance of Mode 4 can be calculated using equation (8), which is a revised version of equation (3) (replacing g by p).

$$F_{ps\ 4} = 4\pi M_p \times \left(1 + \frac{R_s + r}{R_s}\right) + 4M_p \times \left(\frac{2p - 2r}{R_s + r}\right) \tag{8}$$

- **Mode 5**

Figure 4 , e shows the yield patterns for Mode 5. Four quarters of the fan yield mechanism are distributed at the corners of the yielded area. In addition, there are eight connecting yield lines. Equation (9) represents the plastic resistance of the SHS plate of Mode 5.

$$F_{ps\ 5} = 2\pi M_p \times \left(1 + \frac{R_s + r}{R_s}\right) + 2M_p \times \left(\frac{3p + 3g - 4r}{R_s + r}\right) \tag{9}$$

- **Mode 6**

Mode 6 differs from Mode 5 in that it has only straight yield lines with no fan yielding (Figure 4, f). Equation (10) is the plastic resistance of the SHS plate for Mode 6. The unknown dimension y can be determined using equation (6).

$$F_{ps\ 6} = 4M_p \times \left(\frac{g + 2R_s + r}{y + r} + \frac{p + 2y + r}{R_s}\right) \tag{10}$$

The plastic resistance formulas for the SHS plate were divided into two groups. The first for those with very large bolt pitch to represent two single rows working individually and it includes Mode 1, Mode 2 and Mode 3. The second group for the cases with small bolt pitch to demonstrate the group of two rows working together, and it includes Mode 4, Mode 5 and Mode 6. The formulas of the plastic resistance for the SHS plate, that were derived previously, were applied to the whole range of SHS that could be used as compression members to specify the dominating yielding modes. The yielding strength for all sections was assumed to equal 355N/mm². The minimum centre-to-centre spacing between EHBs and the maximum bolt gauge distance were chosen to satisfy the requirements for practical concrete placement around the anchorage. The results demonstrate that Mode 2 and Mode 5 are always dominating the behaviour of the SHS plate for the whole range of SHS that could be used as compression members. Therefore, Mode 2 (for rows acting independently) and Mode 5 (for rows acting together) are adopted for developing the analytical model for plastic resistance of the column face component. Figure 5 illustrates the results of the proposed model for some of the square hollow sections. These Figures represent samples to demonstrate how Mode 2 and Mode 5 dominate the SHS plate behaviour.
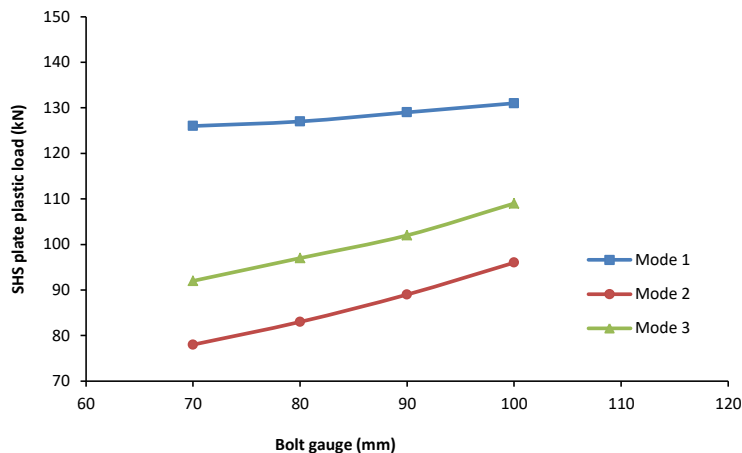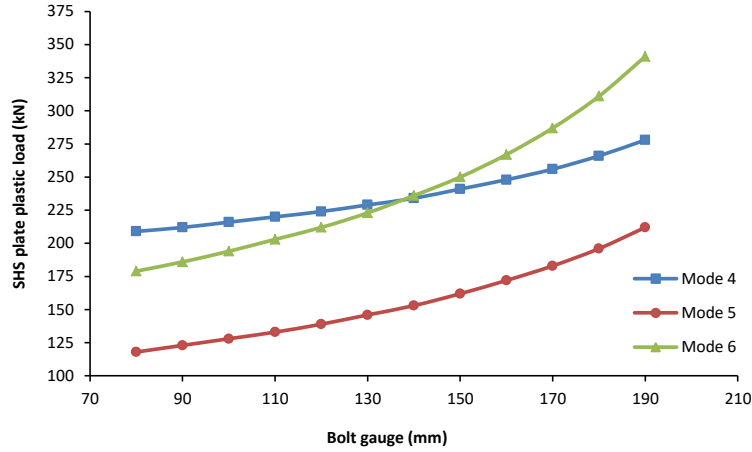

(a) SHS200×200×5 (two rows acting independently)

7
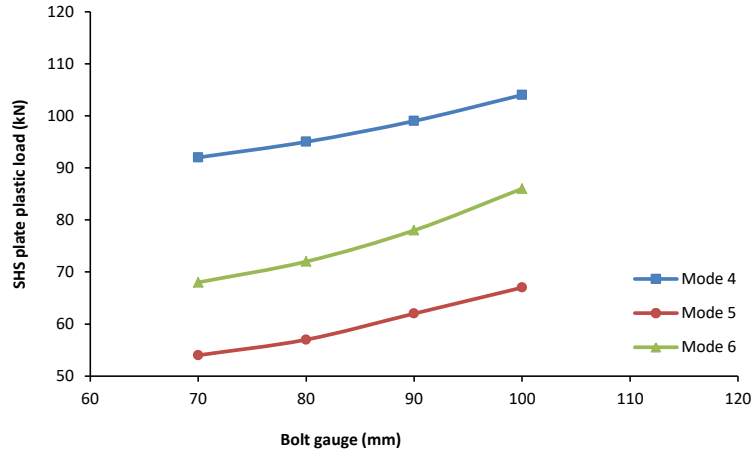
(b) SHS200×200×5, p =120mm (two rows acting together)
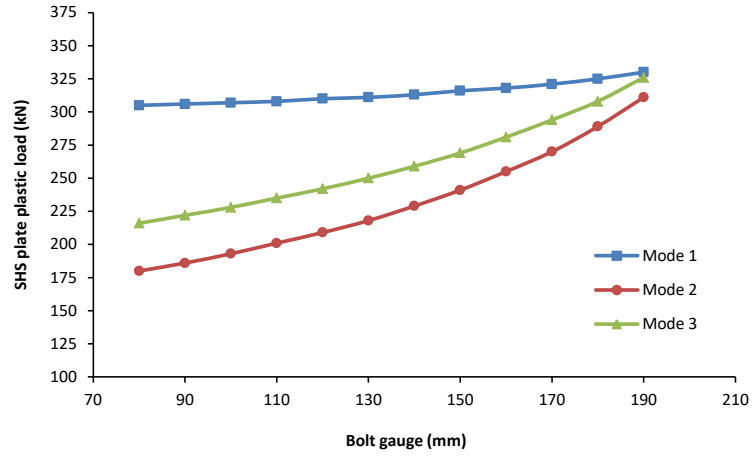
(c) SHS300×300×8 (two rows acting independently)

(d) SHS300×300×8, p =150mm (two rows acting together)

Figure 5: Plastic load of SHS plate

It is clear that the bolt pitch (p) is the key factor, which can change the yielding pattern from Mode 2 to Mode 5. This means there is a critical value for the bolt pitch (p_{crt}). Mode 2 exists in connections with bolt pitch larger than p_{crt}, whereas for p smaller than p_{crt} the yielding mechanism changes into one group of four bolts acting together (Mode 5). To find a relationship that could be used to calculate p_{crt} for Mode 2 and Mode 5, it is assumed that at the critical bolt pitch the plastic resistance for the SHS plate of Mode 2 and Mode 5 are equal. So equating equations (3) and (9) provides:

$$p_{crt\,SHS} = \frac{\pi}{3} \times (R_s + r)\left(1 + \frac{R_s + r}{R_s}\right) + \frac{g}{3} \qquad (11)$$

8

Applying equation (11) on 200×200×6.3 SHS with a bolt gauge of 80 mm states that Mode 5 exists for connections with bolt pitches larger than 169mm. The parametric study of Mahmood [29] for the same section showed that connections with bolt pitches equal to or higher than 160mm fail in a mechanism similar to Mode 5. This means equation (11) provides a fair estimation for the critical bolt pitch. Figure 6 demonstrates the effect of bolt pitch on changing the yielding mechanism from Mode 2 to Mode 5.
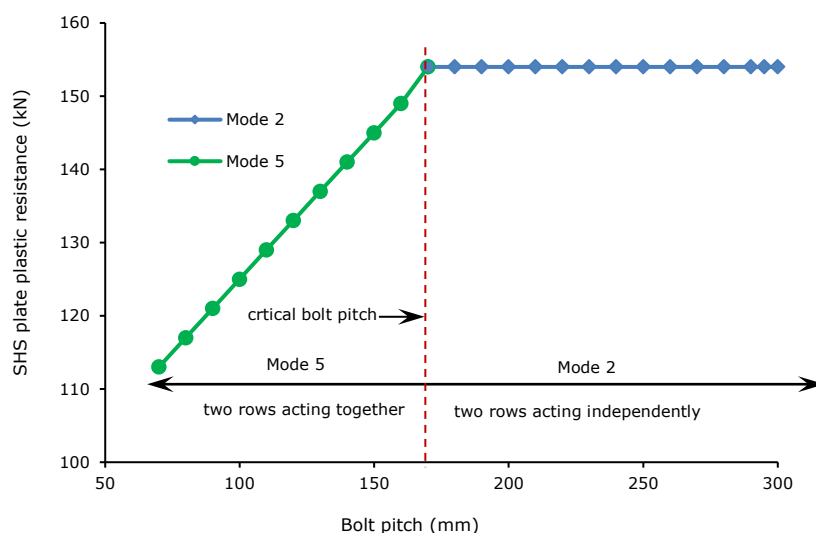

Figure 6: Specifying the critical bolt pitch (SHS200×200×6.35, g=80mm)

3.2. EHB anchorage resistance

Previous studies on the EHB connections showed that the anchorage fails by pulling-out a concrete cone [26, 29]. This kind of failure is due to the concrete tensile cracking across the failure surface [30, 31]. Thus, the anchored pull-out strength (F_{pa}) depends on the cracked area and the concrete strength. The cracked area can be considered as the projected area of the failure cone at the concrete surface [32, 33]. Figure 7 presents the concrete cone failure mechanism and the projected area.
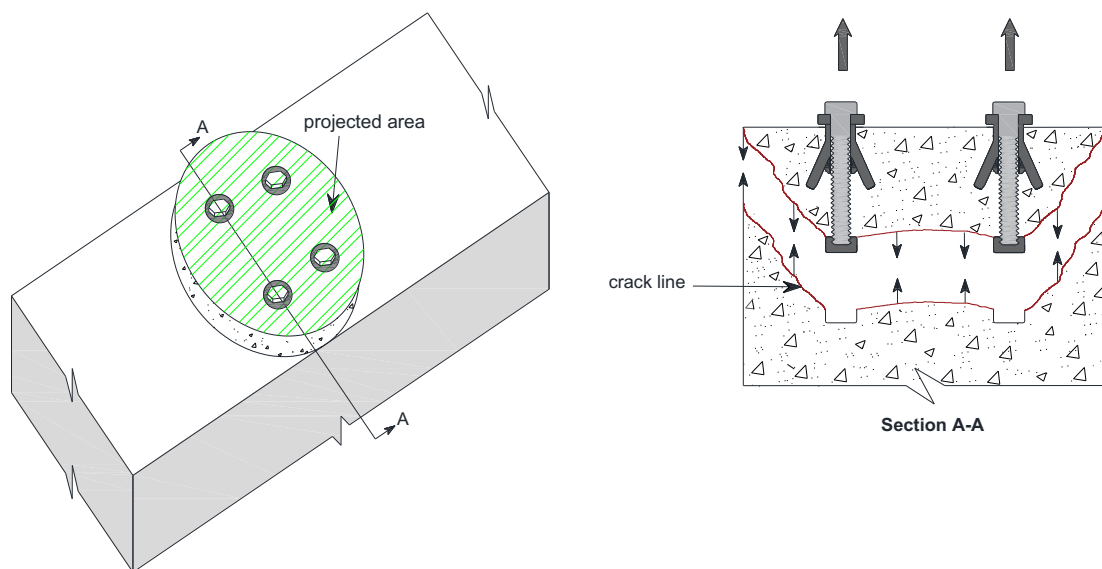

Figure 7: Pull-out concrete cone failure

The anchorage plastic resistance is

$$F_{pa} = A_c \times f_{tc} \tag{12}$$

where

9

A_c: concrete cone projected area and it can be calculated based on the cone failure mode.

f_{tc}: confined concrete tensile strength.

In this study, the square root relationship between the concrete compressive and tensile strengths overestimates the cone pull-out capacity in the range of low and normal strength concrete. This finding matches what was stated by Werner Fuchs and John [31]. Therefore, the concrete tensile strength (f_{ct}) is considered equal to 10% of the characteristic concrete cubes compressive strength (f_{cu}).

Tizani et al. [26] suggested equation (13) to consider the confinement effect of SHS on the concrete strength.

$$\gamma_2 = \frac{f_y}{10\mu} \quad \geq \quad 1 \tag{13}$$

where

μ : column face slenderness ratio $= \dfrac{b}{t}$

Accordingly, equation (14) can be used to calculate the confined concrete tensile strength.

$$f_{ct} = 0.1 \times f_{cu} \times \gamma_2 \tag{14}$$

Figure 8 shows the possible anchorage failure modes. Mode I is EHB connection with only two bolts in tension. Modes II and III characterise EHB connections of two rows of bolts in tension with large and small bolt pitch respectively. Mode II exists for connections with a bolt pitch equal to or larger than the critical concrete bolt pitch distance ($p_{crt\ con}$). Mahmood [29] suggested equation (15) to estimate $p_{crt\ con}$.

$$p_{crt\ con} = 2.39\ L_{an} \tag{15}$$
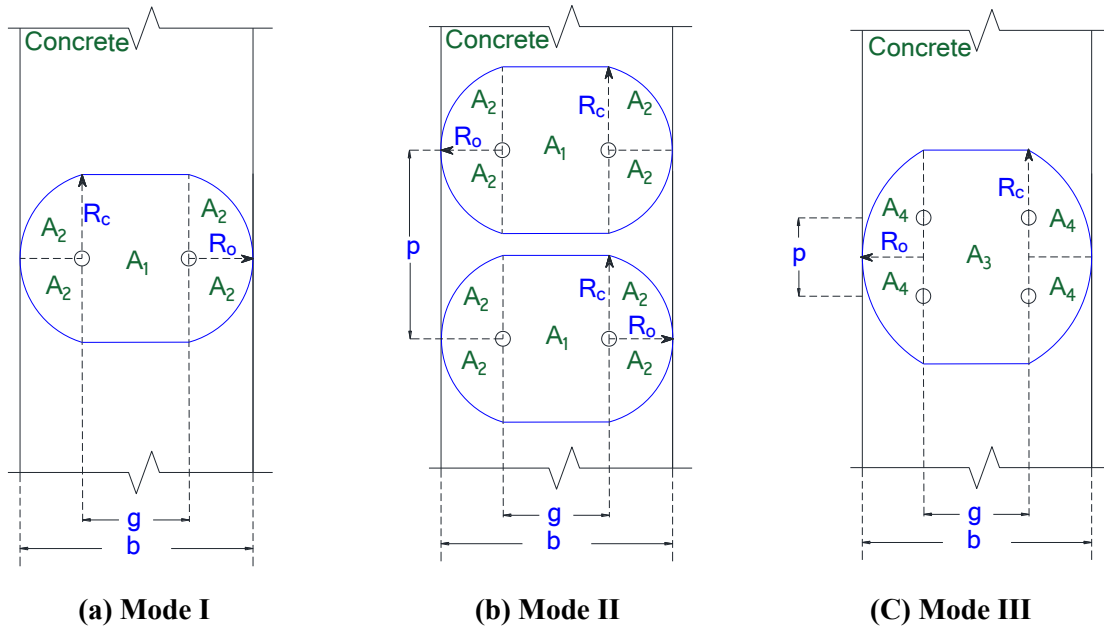

(a) Mode I   (b) Mode II   (C) Mode III

Figure 8: Concrete cone failure modes

The calculation of A_c depends on the cone failure mode, which could be one of the following modes:

Mode I (Figure 8, a)**:** single row of two EHBs.

$$A_c = A_1 + 4A_2$$

$$A_{c\ I} = 2R_c \times g + \frac{8}{3} \times R_c \times R_o \tag{16}$$

R_c is the radius of the concrete cone at the plastic resistance and it can be calculated using equation (17) [26].

$$R_c = 0.82 \times L_{an} \tag{17}$$

The distance from the bolt centreline to the concrete edge is defined as R_0, and it can be calculated as follows:

$$R_o = \frac{b - g - 2t}{2} \tag{18}$$

Mode II (Figure 8, b)**:** two rows of two EHBs acting independently. This is the case when the bolt pitch is larger than $p_{crt\,con}$ so that there is clear undamaged concrete between the two rows. The concrete cone projected area for this mode is supposed to be double that for Mode I. However, it is found that this assumption underestimates the anchored strength, which means it is less than the actual cracked area. Therefore, the geometrical coefficient γ_3 (equation (22)) is proposed to calculate the projected area for this mode (equation (19)).

$$A_{c\,II} = \gamma_3 \left[2R_c \times g + \frac{8}{3} \times R_c \times R_o \right] \tag{19}$$

Mode III (Figure 8, c): two rows of two EHBs acting together in the case of small bolt pitch so that there is complete damage of the concrete between the two rows. It is assumed that connections with bolt pitch less than $p_{crt\,con}$ are considered to fail in Mode III.

$$A_c = A_3 + 4A_4$$

$$A_{c\,III} = (2R_c + p) \times g + \frac{8}{3} \times (R_c + \frac{p}{2}) \times R_o \tag{20}$$

To derive a formula for γ_3 it is assumed that the projected areas for Mode II and Mode III are equal when the bolt pitch is equal to the critical concrete bolt pitch.

Replacing the bolt pitch in equation (20) by the critical bolt pitch from equation (15) provides:

$$A_{c\,III\,@\,pcrt\,con} = (2R_c + 2.39\,L_{an}) \times g + \frac{8}{3} \times (R_c + 1.195\,L_{an}) \times R_o \tag{21}$$

Equating equations (19) and (21) leads to the following expression, which could be used to calculate γ_3:

$$\gamma_3 = \frac{4.03\,g + 5.37\,R_o}{1.64\,g + 2.19\,R_o} \tag{22}$$

4. Validation of the component bending strength model

The behaviour of the column face component in EHB connections is affected by the infill concrete strength, SHS plate thickness (slenderness ratio; $\mu = b/t$), bolt gauges distance, bolt pitches distance, anchorage length of EHB inside the concrete and SHS plate strength. The sensitivity of the proposed model to each of these parameters is validated in this section by comparing the results of the model with the available data in the literature [26, 29]. The proposed model provides a reasonable prediction of the component plastic resistance with a maximum value of the coefficient of variation of 0.05 (Tables 1 to 5). Figure 9 presents a flowchart for determining the plastic resistance of EHB component in bending.

Table 1: Plastic resistance model validation (effect of concrete strength): single row of two EHBs, $f_y=413N/mm^2$, $b=200mm$, $t=6.3mm$, g and $L_{an}=80mm$

f_{cu} (N/mm^2)	Plastic resistance (kN)		$F_{p\ proposed}$ / $F_{p\ [26]}$
	$F_{p\ [26]}$	$F_{p\ proposed}$	
24	150.29	151.56	1.01
25	152.79	154.38	1.01
30	168.41	168.49	1.00
35	183.60	182.59	0.99
36	190.43	185.41	0.97
40	197.02	196.69	1.00
45	212.17	210.79	0.99
50	227.73	224.90	0.99
55	242.66	239.00	0.98
60	257.63	253.10	0.98
65	272.55	267.20	0.98
70	288.57	281.30	0.97
75	302.68	295.41	0.98
80	318.30	309.51	0.97
85	337.72	323.61	0.96
90	347.69	337.71	0.97
Mean			0.99
Standard deviation			0.01
Coefficient of variation			0.01

Table 2: Plastic resistance model validation (effect of column face slenderness ratio): single row of two EHBs, $f_{cu}=40N/mm^2$, $b=200mm$, g and $L_{an}=80mm$

μ (b/t)	f_y (N/mm^2)	Plastic resistance (kN)		$F_{p\ proposed}$ / $F_{p\ [26]}$
		$F_{p\ [26]}$	$F_{p\ proposed}$	
25	406	248.81	271.68	1.09
31.75	413	197.02	196.69	1.00
40	445	151.23	154.50	1.02
Mean				1.04
Standard deviation				0.05
Coefficient of variation				0.05

Table 3: Plastic resistance model validation (effect of bolt gauge): single row of two EHBs,
$f_y=454N/mm^2$, $f_{cu}=40N/mm^2$, $b=300mm$, $t=8mm$ and $L_{an}=80mm$

| g (mm) | Plastic resistance (kN) | | $F_{p\ proposed}$ / F_p |
	$F_{p\ [29]}$	$F_{p\ proposed}$	[29]
80	175.01	183.39	1.05
90	179.17	187.80	1.05
100	183.34	192.49	1.05
110	187.51	197.52	1.05
120	191.67	202.94	1.06
130	195.84	208.83	1.07
140	200.01	215.27	1.08
150	212.75	222.38	1.05
160	228.81	230.30	1.01
170	247.53	239.23	0.97
180	256.04	249.42	0.97
Mean			1.04
Standard deviation			0.04
Coefficient of variation			0.04

Table 4: Plastic resistance model validation (effect of anchorage length): single row of two EHBs,
$f_y=407N/mm^2$, $f_{cu}=40N/mm^2$, $b=300mm$, $t=10mm$, $\mu=31.75$ and $g=80mm$

| L_{an} (mm) | Plastic resistance (kN) | | $F_{p\ proposed}$ / F_p |
	$F_{p\ [29]}$	$F_{p\ proposed}$	[29]
80	230.09	227.57	0.99
85	233.43	240.38	1.03
90	237.42	253.54	1.07
95	245.78	267.05	1.09
100	265.85	280.91	1.06
103	274.85	289.39	1.05
105	291.79	295.12	1.01
110	325.86	309.67	0.95
112	342.84	315.64	0.92
Mean			1.02
Standard deviation			0.06
Coefficient of variation			0.05

Table 5: Plastic resistance model validation (effect of bolt pitch): double rows of two EHBs,
$f_y=413N/mm^2$, $f_{cu}=40N/mm^2$, $b=200mm$, $t=6.3mm$, g and $L_{an}=80mm$

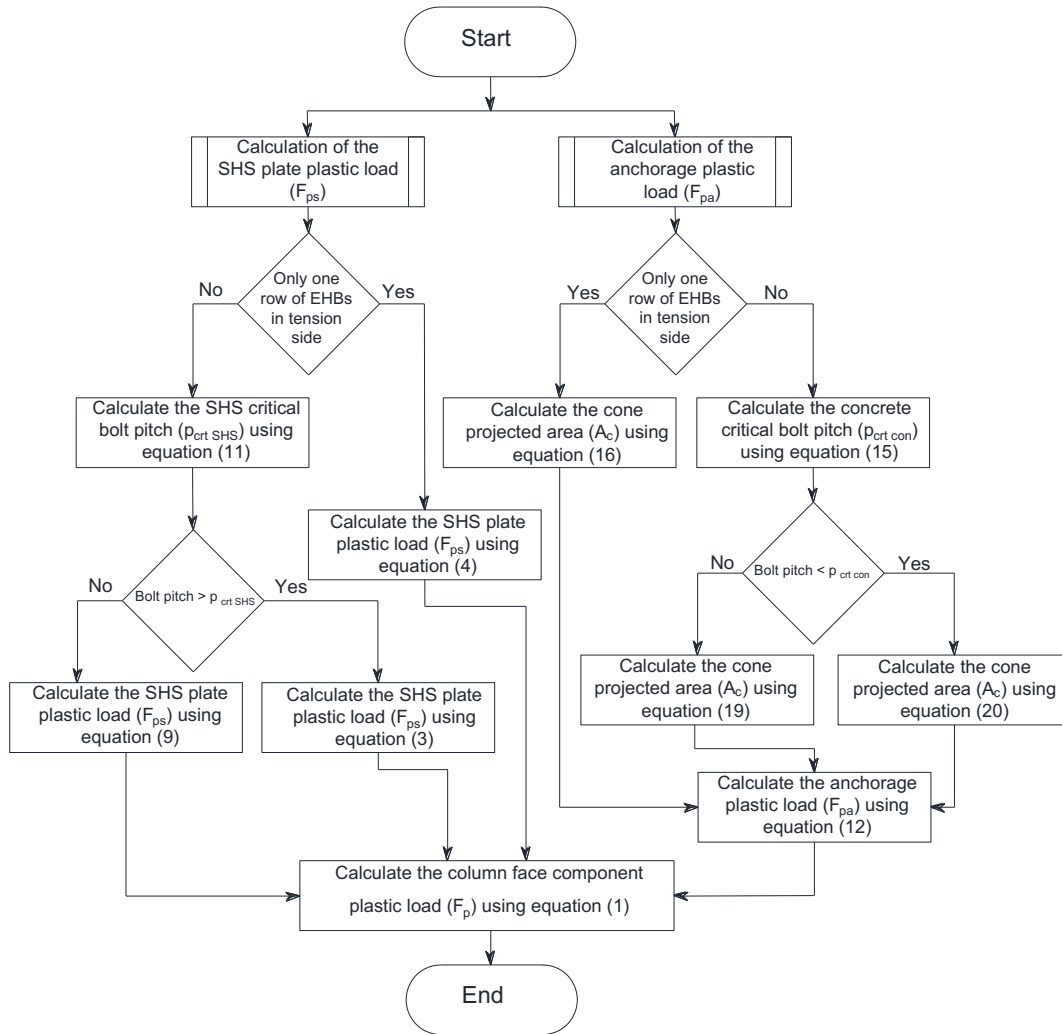| p (mm) | Plastic resistance (kN) | | $F_{p\ proposed}$ / F_p |
	$F_{p\ [29]}$	$F_{p\ proposed}$	[29]
120	348.81	361.52	1.04
140	361.12	387.65	1.07
150	372.78	400.72	1.07
160	377.87	418.15	1.11
180	389.49	435.00	1.12
190	402.09	443.94	1.10
200	406.69	444.69	1.09
210	407.66	444.69	1.09
220	411.02	444.69	1.08
240	411.27	444.69	1.08
260	412.73	444.69	1.08
280	412.91	444.69	1.08
Mean			1.09
Standard deviation			0.01
Coefficient of variation			0.01

Figure 9: Flowchart for determining the component plastic resistance

5. Column face initial bending stiffness

The column face component is represented as four parallel springs; one at each bolt location (Figure 10, a). To calculate the initial stiffness of the column face component (k_i) the following assumptions were adopted: the material is linear elastic and in-plane deformations are negligible. Since the springs are acting in parallel, the effective stiffness of the column face component would be the summation of the four sprigs stiffness (Figure 10, b).
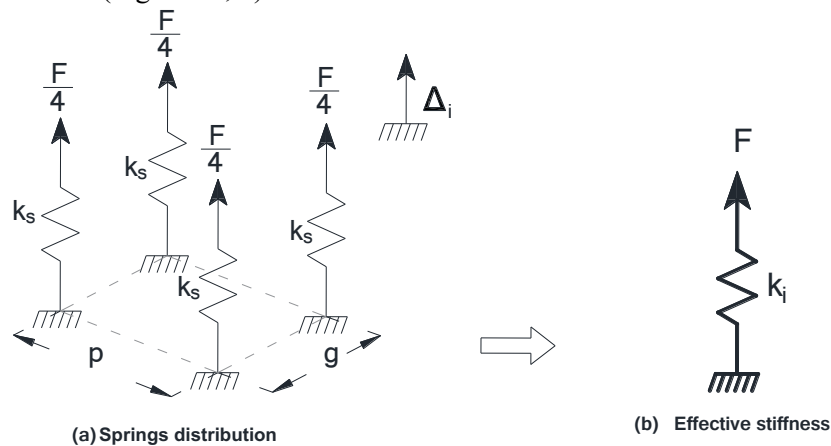

(a) Springs distribution

(b) Effective stiffness

Figure 10: Equivalent spring model for column face component

$$k_i = 4k_s \tag{23}$$

14

where

k_i: the initial stiffness of the column face component

k_s: spring stiffness

$$k_s = \frac{F}{4\Delta_s}$$

(24)

where

F: the total applied force on the component

Δ_s: spring displacement; which represents the column face displacement at bolt location

Equation (24) suggests that the spring stiffness could be determined once the spring displacement is calculated in terms of the total applied force (F). Ghobarah et al. [3], proposed equation (25) to calculate the column face displacement at bolt location for concrete-filled SHS connected by four high strength blind bolts.

$$\Delta_s = \frac{12\gamma_f \times F \, (b - 2t)^2 \, (1 - v^2)}{E_s \times t_{eq}^3}$$

(25)

where

γ_f: deflection coefficient

b: SHS width

t: SHS plate thickness

v: SHS Poison's ratio

E_s: Young modulus of elasticity for SHS

t_{eq}: equivalent column face component thickness

Substituting equation (25) in equation (24) provides

$$k_s = \frac{E_s \times t_{eq}^3}{48 \times \gamma_f \times (b - 2t)^2 \times (1 - v^2)}$$

(26)

The initial stiffness of the column face component can be calculated using equation (27).

$$k_i = \frac{E_s \times t_{eq}^3}{12 \times \gamma_f \times (b - 2t)^2 \times (1 - v^2)}$$

(27)

Mahmood [29] and Tizani et al. [26] performed extensive studies for a wide range of EHB connections to quantify the effect of the influential parameters on the bending behaviour of the column face component in EHB connections. They stated that the effect of bolt pitch on initial stiffness is negligible and the initial stiffness of the column face component of the double row of EHBs is equivalent to twice of a single row. Accordingly, equation (27) is reproduced here as equations (28) and (29).

$$k_{i \, single} = \frac{E_s \times t_{eq}^3}{24 \times \gamma_f \times (b - 2t)^2 \times (1 - v^2)}$$

(28)

$$k_{i \, double} = \frac{E_s \times t_{eq}^3}{12 \times \gamma_f \times (b - 2t)^2 \times (1 - v^2)}$$

(29)

where

$k_{i \, single}$: initial stiffness for single row of two EHBs

$k_{i \, double}$: initial stiffness for double rows of two EHBs each

The calculation of k_i requires defining the equivalent component thickness (t_{eq}) and the deflection coefficient (γ_f). In this study, the effect of the infill concrete strength and the bolt anchored length are considered as an additional thickness to the column face plate. This assumption is in agreement with the findings of France et al. [25], which stated that the use of concrete infill can be counted as an increase

15

in the thickness of the column plate. Hence, the following equation is proposed to calculate the equivalent component thickness.

$$t_{eq} = f_{cu} \times \lambda_{f_{cu}} + L_{an} \times \lambda_{L_{an}} + t \tag{30}$$

where

t_{eq} : the equivalent thickness of the column face component in millimetres

f_{cu} : characteristic concrete cubes compressive strength in N/mm^2

$\lambda_{f_{cu}}$: rate of change in the component stiffness due to varying f_{cu} (Table 6)

L_{an} : EHB anchored length in millimetres

$\lambda_{L_{an}}$: rate of change in the component stiffness due to varying L_{an} (Table 7)

t : the thickness of the SHS plate in millimetres

Mahmood [29] and Tizani et al. [26] confirmed that there is negligible change in the component initial stiffness when increasing the concrete strength to more than 50N/mm^2 and using anchorage length longer than (105mm) 6.5 times the bolt. Consequently, the coefficients $\lambda_{f_{cu}}$ and $\lambda_{L_{an}}$ are calculated based on the amount of variation in the component initial stiffness with the change of concrete strength and bolt anchored length respectively (tables 6 and 7).

Table 6: Effect of concrete strength on component stiffness [26]

Concrete strength (N/mm^2)	Component initial stiffness (kN/mm)	Rate of improvement in component initial stiffness (Δk_i)	Change in concrete strength (Δf_{cu}) (N/mm^2)	$\lambda_{f_{cu}}$ (Δk_i / Δf_{cu})
25	202	0.38	25	0.015
50	279			

Table 7: Effect of bolt anchored length on component stiffness [29]

Anchored length (mm)	Component initial stiffness (kN/mm)	Rate of improvement in component initial stiffness (Δk_i)	Change in anchored length (ΔL_{an}) (mm)	$\lambda_{L_{an}}$ (Δk_i / ΔL_{an})
80	183	0.20	25	0.008
105	220			

Substituting the values of $\lambda_{f_{cu}}$ and $\lambda_{L_{an}}$ in equation (30) provides the following equation to calculate the equivalent component thickness:

$$t_{eq} = 0.015\, f_{cu} + 0.008\, L_{an} + t \tag{31}$$

where $f_{cu} \leq 50$ N/mm^2 and $L_{an} \leq 105$mm.

Ghobarah et al.[3] calculated the deflection coefficient by considering the bolt gauge distance, the bolt pitch distance and the SHS geometry. As stated earlier, the variation of the bolt pitch distance has a negligible effect on the component initial stiffness [29]. Therefore, only the bolt gauge distance and the geometry of the SHS are included in calculating the deflection coefficient. The finite element model that was used by Tizani et al. [26] was employed to find the component displacement at 0.75 of its plastic resistance (Δ_i). The analyses were performed for components with different slenderness ratios and bolt gauges. Equation (32), which was reproduced from equation (25) was used to calculate γ_f. Then the results were used to produce the chart presented in Figure 11. This chart can be used to calculate the deflection coefficient.

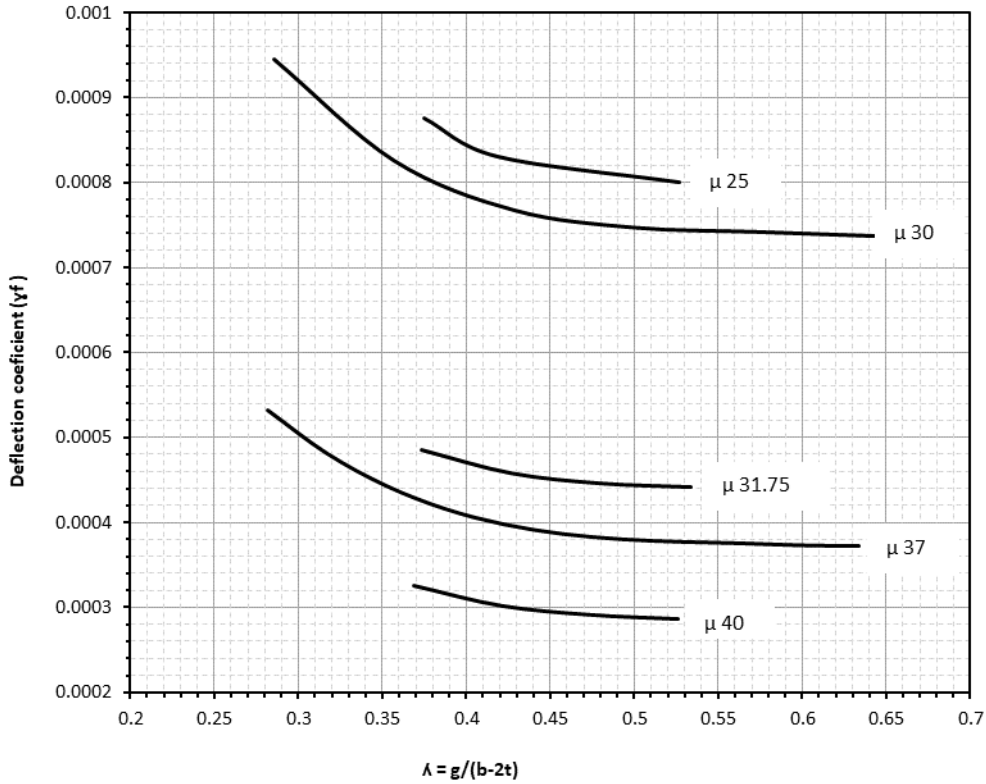$$\gamma_f = \frac{\Delta_i \times E_s \times t_{eq}^3}{24 \times 0.75 F_p \, (b - 2t)^2 \, (1 - v^2)} \qquad\qquad (32)$$

Figure 11: Deflection coefficient (γ_f)

6. Validation of the column face initial bending stiffness

To evaluate the accuracy of the proposed model, its results were compared with the available data in the literature [26, 29]. Tables 8 to 12 show that the proposed model provides a fair estimation of the component initial stiffness with a maximum value of the coefficient of variation equal to 0.08.

Table 8: Initial stiffness model validation (effect of concrete strength): single row of two EHBs, f_y=413N/mm², b=200mm, t =6.3mm, g and L_{an} =80mm

f_{cu} (N/mm²)	Initial stiffness (kN/mm)		$k_{i \text{ proposed}} / k_{i \, [26]}$
	$k_{i \, [26]}$	$k_{i \text{ proposed}}$	
24	192	212	1.10
25	202	213	1.05
30	225	220	0.98
35	246	227	0.92
36	259	228	0.88
40	263	234	0.89
45	275	241	0.88
50	279	250	0.90
55	280	250	0.89
60	281	250	0.89
65	283	250	0.88
70	283	250	0.88
75	284	250	0.88
80	284	250	0.88
85	285	250	0.88
90	286	250	0.87
Mean			0.92
Standard deviation			0.07
Coefficient of variation			0.08

Table 9: Initial stiffness model validation (effect of component slenderness ratio): single row of two EHBs, f_{cu}=40N/mm^2, b=200mm, g and L_{an} =80mm

μ (b/t)	Initial stiffness (kN/mm)		$k_{i\ proposed}$ / $k_{i\ [26]}$
	$k_{i\ [26]}$	$k_{i\ proposed}$	
25	264	267	1.01
31.75	241	234	0.97
40	189	188	0.99
Mean			0.99
Standard deviation			0.02
Coefficient of variation			0.02

Table 10: Initial stiffness model validation (effect of bolt gauge): single row of two EHBs, f_y=454N/mm^2, f_{cu}=40N/mm^2, b=300mm, t =8mm and L_{an} =80mm

g (mm)	Initial stiffness (kN/mm)		$k_{i\ proposed}$ / $k_{i\ [29]}$
	$k_{i\ [29]}$	$k_{i\ proposed}$	
80	195	174	0.89
90	219	192	0.88
100	231	209	0.90
110	248	222	0.90
120	263	233	0.89
130	270	240	0.89
140	276	243	0.88
150	278	245	0.88
160	281	247	0.88
170	282	248	0.88
180	283	249	0.88
Mean			0.89
Standard deviation			0.01
Coefficient of variation			0.01

Table 11: Initial stiffness model validation (effect of anchorage length) : single row of two EHBs, f_y=407N/mm^2, f_{cu}=40N/mm^2, b=300mm, t =10mm, μ=31.75 and g =80mm

L_{an} (mm)	Initial stiffness (kN/mm)		$k_{i\ proposed}$ / $k_{i\ [29]}$
	$k_{i\ [29]}$	$k_{i\ proposed}$	
80	183	178	0.97
85	188	180	0.96
90	191	182	0.95
95	199	184	0.92
100	210	186	0.89
103	219	187	0.85
105	220	188	0.85
110	218	188	0.86
112	218	188	0.86
Mean			0.90
Standard deviation			0.05
Coefficient of variation			0.05

Table 12: Initial stiffness model validation (effect of bolt pitch) : double rows of two EHBs, $f_y=413N/mm^2, f_{cu}=40N/mm^2, b=200mm, t=6.3mm, g$ and $L_{an}=80mm$

p (mm)	Initial stiffness (kN/mm)		$k_{i\ proposed}$ / $k_{i\ [29]}$
	$k_{i\ [29]}$	$k_{i\ proposed}$	
120	465	467	1.00
140	478	467	0.98
150	476	467	0.98
160	490	467	0.95
180	490	467	0.95
190	498	467	0.94
200	496	467	0.94
210	498	467	0.94
220	497	467	0.94
240	496	467	0.94
260	492	467	0.95
280	494	467	0.95
Mean			0.95
Standard deviation			0.02
Coefficient of variation			0.02

7. The overall behaviour of the component

The analyses of the data presented by Tizani et al. [26] and Mahmood [29] reveals that the column face bending behaviour can be divided into four stages: initial, secondary, drop and membrane action stages. Accordingly, a quad-linear model (Figure 12) is proposed in this study to simulate the bending behaviour of the column face component in EHB connections for all these stages. Tizani et al. [26] and Mahmood [29] reported that the linear behaviour of the component (the initial stage in the proposed model) extends to 75% of the component plastic resistance. The secondary stage covers the behaviour between 75% of the plastic load and the plastic load. The drop in the component resistance after the plastic load to the lowest load before the component strength starts picking up is termed as the drop stage. The final stage is the membrane action stage in which the component strength starts increasing due to the membrane action in the steel plate. The statistical analysis reported by Mahmood [29] showed that the stiffness of the secondary stage (k_{se}) and of the membrane action stage (k_m) can be presented as a ratio of the initial stiffness of the component (k_i). Thus, in this study k_{se} and k_m are considered equivalent to *17%* and 2% of k_i respectively. This assumption is accepted in the research community and many researchers presented the post yield stiffness as a percentage of the initial stiffness [3, 13]. Likewise, the mean value of the ratio of the drop displacement (Δ_d) to the displacement at the plastic load (Δ_p) is used to calculate the drop displacement. The following equations are proposed to meet the previous assumptions to calculate the characteristics of the quad-linear model.

$$k_i = \frac{0.75F_p}{\Delta_i} \tag{33}$$

$$k_{se} = \frac{0.25F_p}{\Delta_p - \Delta_i} = 0.17k_i \tag{34}$$

$$k_d = \frac{F_d - F_p}{\Delta_d - \Delta_p} \tag{35}$$

$$k_m = \frac{F_u - F_d}{\Delta_u - \Delta_d} = 0.02k_i \tag{36}$$

$$\Delta_d = 3.5\,\Delta_p \tag{37}$$

where:

k_i : initial stiffness of the column face component

Δ_i : column face displacement at *0.75F$_p$*

k_{se} : secondary stiffness of the column face component

Δ_p : column face displacement at F_p

F_p : plastic strength of the column face component

k_d : drop stiffness of the column face component

Δ_d : column face displacement at F_d

F_d : lowest strength of the column face component after the plastic load

k_m : membrane action stiffness of the column face component

Δ_u : column face displacement at F_u
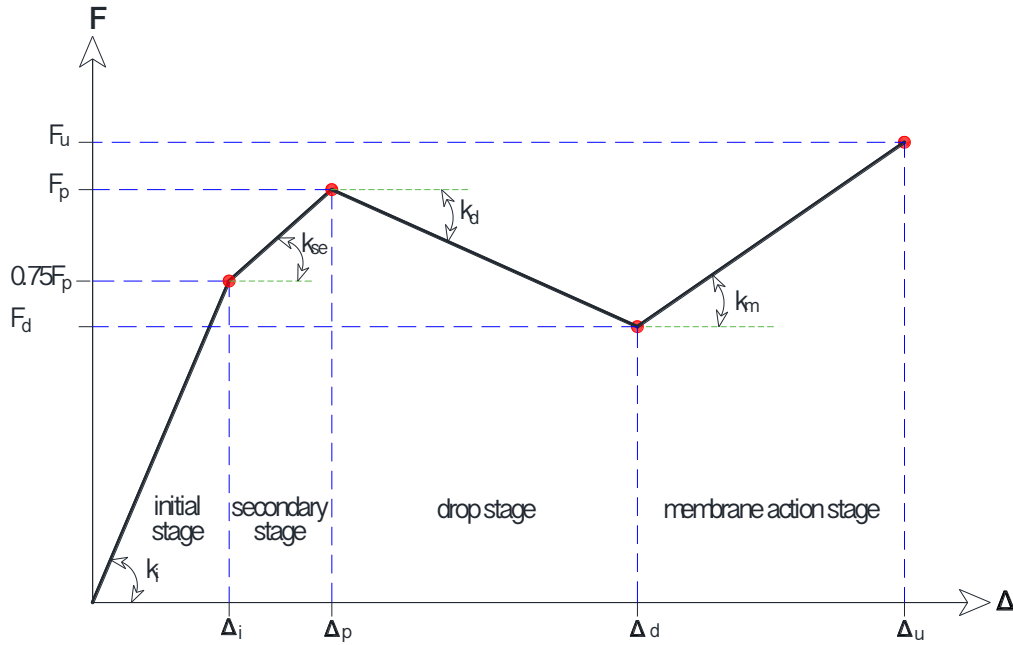
F_u : ultimate column face strength

Figure 12: Quad-linear model for bending behaviour of the column face component

The drop stiffness (k_d) can be calculated using equation (35). However, it requires knowing the value of the drop load (F_d). Mahmood [29] proposed equation (38) to calculate F_d.

$$F_d = F_p \left(1.0734 \times e^{-0.178\left(\frac{F_{pa}}{F_{ps}}\right)} \right) \tag{38}$$

where:

F_p: column face component plastic load, equation (1)

F_{pa}: anchorage plastic load, equation (12)

F_{ps}: SHS plate plastic load, equations (3) or (4) or (9)

Considering that F_p and k_i can be calculated from the analytical model that have been developed in this study, the proposed quad-linear model results versus the data from Mahmood [4] and Tizani et al. [9] are plotted in Figure 13. The proposed model shows good agreement with these data.
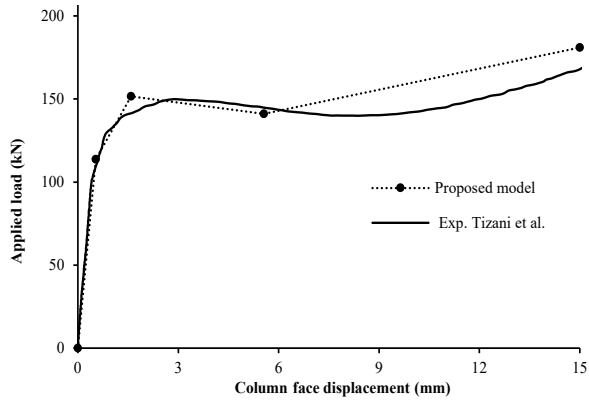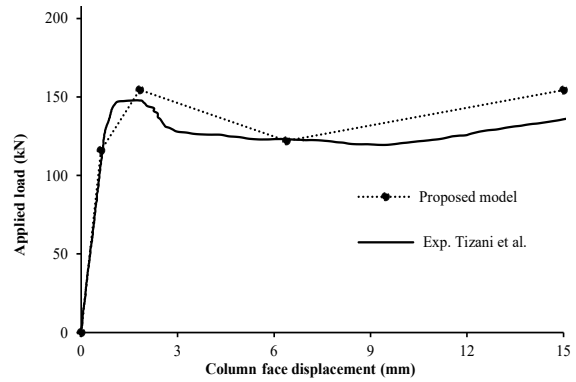
(a) single row of two EHBs, $E_s = 191000N/mm^2$, $f_y=413N/mm^2$, $f_{cu}=24N/mm^2$, $b =200mm$, $t =6.3mm$, g and $L_{an} =80mm$
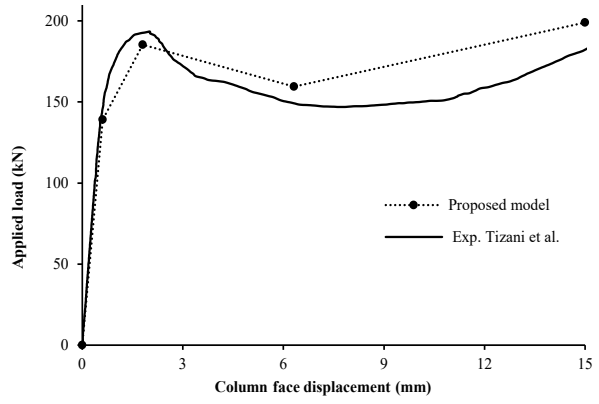
(b) single row of two EHBs, $E_s = 191000N/mm^2$, $f_y=413N/mm^2$, $f_{cu}=36N/mm^2$, $b =200mm$, $t =6.3mm$, g and $L_{an} =80mm$
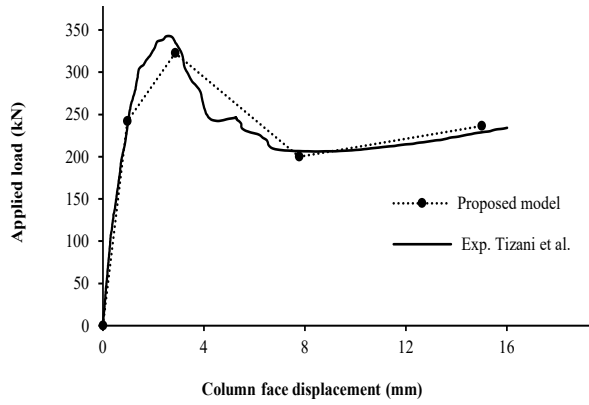
(c) single row of two EHBs, $E_s=191000N/mm^2$, $f_y=413N/mm^2$, $f_{cu}=90N/mm^2$, $b=200mm$, $t =6.3mm$, g and $L_{an} =80mm$

(d) single row of two EHBs, $E_s=185000N/mm^2$, $f_{cu}=40N/mm^2$, $b =200mm$, $t =5mm$, g and $L_{an} =80mm$
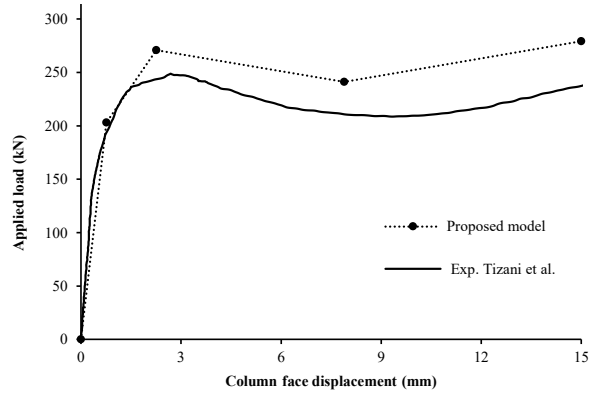
(e) single row of two EHBs, $E_s = 185000N/mm^2$, $f_{cu}=40N/mm^2$, $b =200mm$, $t =8mm$, g and $L_{an} =80mm$
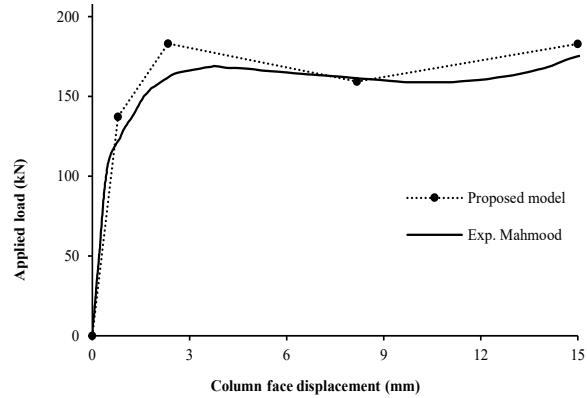
(f) single row of two EHBs, $E_s = 206000N/mm^2$, $f_y = 454N/mm^2$, $f_{cu}= 40N/mm^2$, $b =300mm$, $t = 8mm$, $g = 80mm$ and $L_{an} =80mm$
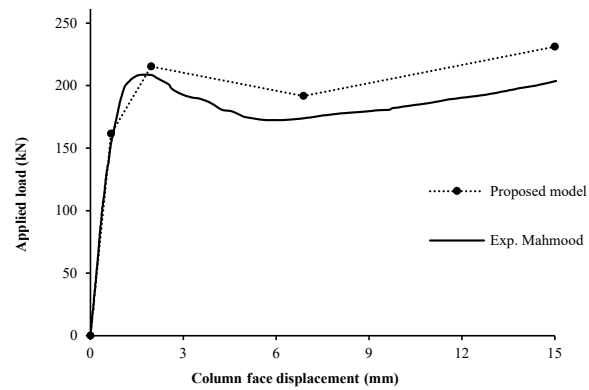
(g) single row of two EHBs, $E_s = 206000N/mm^2$, $f_y =454N/mm^2$, $f_{cu} = 40N/mm^2$, $b = 300mm$, $t = 8mm$, $g = 140mm$ and $L_{an} =80mm$
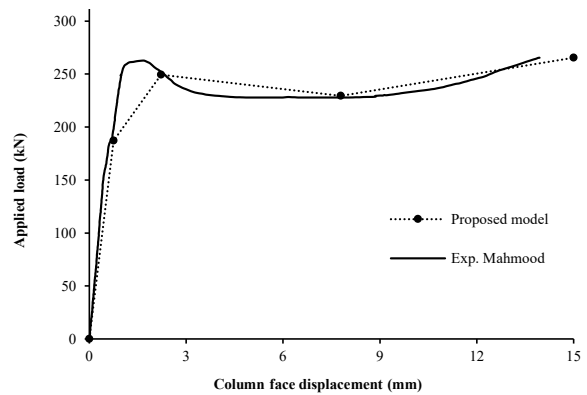
(h) single row of two EHBs, $E_s = 206000N/mm^2$, $f_y =454N/mm^2$, $f_{cu} = 40N/mm^2$, $b = 300mm$, $t = 8mm$, $g = 180mm$ and $L_{an} =80mm$

21

(i) single row of two EHBs, E_s =203000N/mm², f_y =407N/mm², f_{cu} =40N/mm², b = 300mm, t = 10mm, L_{an} = 80mm and g =80mm

(j) single row of two EHBs, E_s =203000N/mm², f_y = 407N/mm², f_{cu} =40N/mm², b = 300mm, t =10mm, L_{an} =103mm and g =80mm

(k) single row of two EHBs, E_s = 203000N/mm², f_y = 407N/mm², f_{cu} = 40N/mm², b = 300mm, t = 10mm, L_{an} =112mm and g =80mm

(l) double rows of two EHBs, E_s =191000N/mm², f_y =413N/mm², f_{cu} =40N/mm², b =200mm, t =6.3mm, p = 120mm, g and L_{an} =80mm

(m) double rows of two EHBs, E_s =191000N/mm², f_y =413N/mm², f_{cu} =40N/mm², b =200mm, t =6.3mm, p = 200mm, g and L_{an} =80mm

(n) double rows of two EHBs, E_s =191000N/mm², f_y =413N/mm², f_{cu} =40N/mm², b =200mm, t =6.3mm, p =280mm, g and L_{an} =80mm
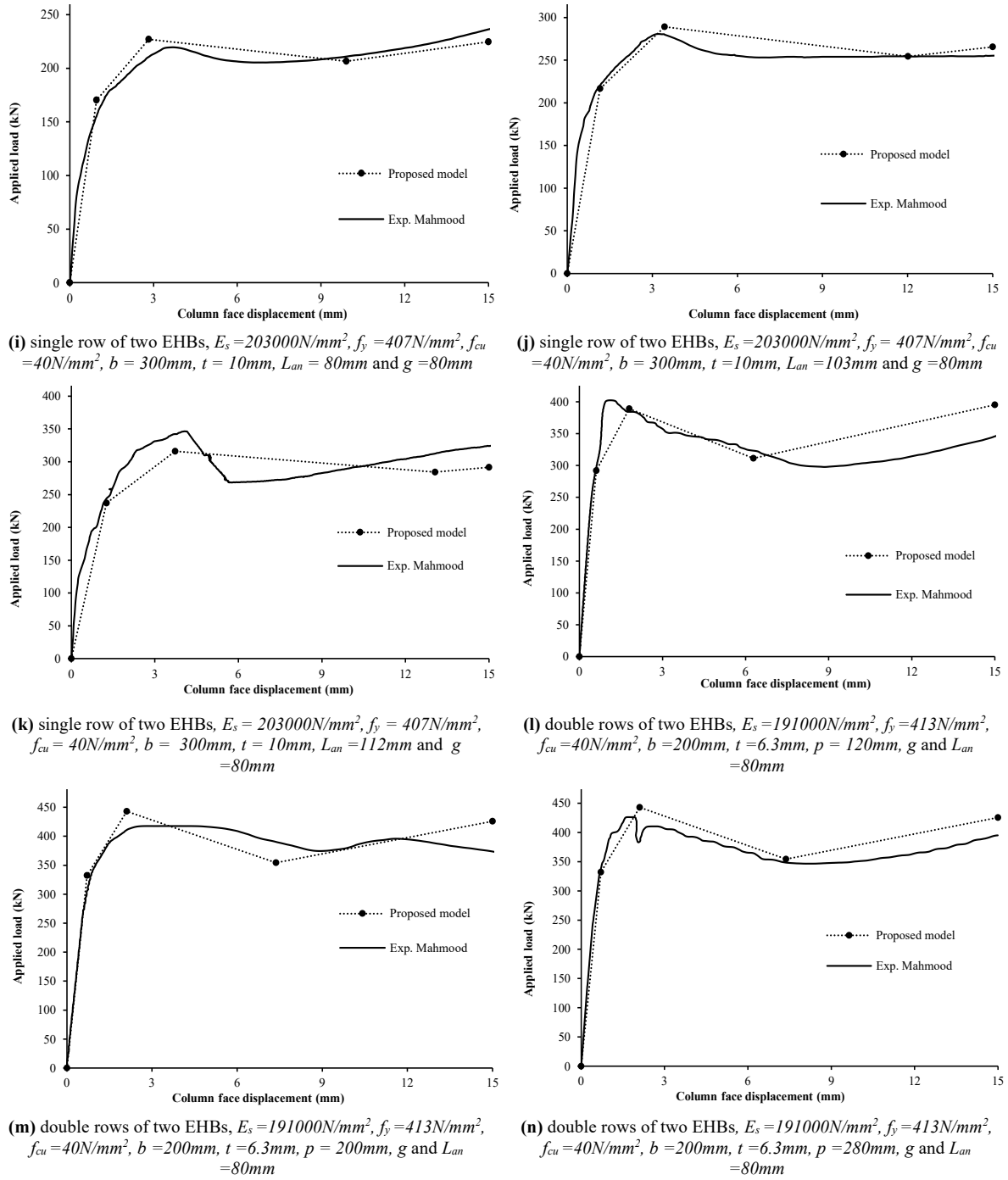
Figure 13: Proposed model vs experimental data.

8. Summary and conclusions

In this study, the bending behaviour of the column face component was analysed as an individual connection component. The results of these analyses were used to propose an analytical model for estimating the main characteristics of the component bending behaviour (plastic resistance and stiffness). The significant parameters that affect the component behaviour are considered resulting in the adequate simulation of the component performance. The proposed model was validated against experimental data and numerical results. The model is quad-linear model to simulate the complete stages of bending behaviour from the initial stage to the membrane action stage. It simulates the component behaviour with an acceptable level of accuracy. The data that were used to validate the proposed model cover the practical range of the EHB connection. The model is a significant step towards the development of design guidance for EHB connections on the basis of the component method.

22

9. Acknowledgements

References

[1] Tizani, W., et al., *Rotational Stiffness of a Blind-Bolted Connection to Concrete-Filled Tubes Using Modified Hollo-Bolt.* Journal of Constructional Steel Research, 2013. **80**: p. 317-331.

[2] Pitrakkos, T. and W. Tizani, *Experimental Behaviour of a Novel Anchored Blind-Bolt in Tension.* Engineering Structures, 2013. **49**: p. 905-919.

[3] Ghobarah, A., S. Mourad, and R.M. Korol, *Moment-Rotation Relationship of Blind Bolted Connections for HSS Columns.* Journal of Constructional Steel Research, 1996. **40**(1): p. 63-91.

[4] Wang, J.F., L.H. Han, and B. Uy, *Behaviour of Flush End Plate Joints to Concrete-Filled Steel Tubular Columns.* Journal of Constructional Steel Research, 2009. **65**(4): p. 925-939.

[5] Lee, J., H.M. Goldsworthy, and E.F. Gad, *Blind Bolted T-Stub Connections to Unfilled Hollow Section Columns in Low Rise Structures.* Journal of Constructional Steel Research, 2010. **66**(8–9): p. 981-992.

[6] Jaspart, J.P., *Recent Advances in the Field of Steel Joints-Column Bases and Further Configurations for Beam-to-Column Joints and Beam Splices*, in *Chercheur qualifié du FNRS, Universite de Liege, Faculte des Sciences Appliques*. 1997, Universite de Liege.

[7] Silva, L., L. Neves, and P. Vellasco, *Design Procedure for I-Beam to Concrete Filled Column and Minor Axis Joints; Characterization of the Component "Column Web Loaded in out-of-Plane Bending"*, in *ECCS Technical Committee 10 "Connections"*. 2004, Deparment of Civil Engineering- University of Coimbra: Coimbra.

[8] Harada, Y., T. Arakaki, and K. MORITA, *Structural Behaviour of RHS Column-to-H Beam Connection with High Strength Bolts.* Steel Structures, 2002. **2**: p. 111-121.

[9] Neves, L. and F. Gomes. *Semi-rigid behaviour of beam-to-column minor-axis joints*. in *IABSE International Colloquium on Semi-Rigid Structural Connections*. 1996. Istanbul, Turkey.

[10] Silva, L., L. Neves, and F. Gomes, *Rotational Stiffness of Rectangular Hollow Sections Composite Joints.* Journal of Structural Engineering, 2003. **129**: p. 487-494.

[11] Elghazouli, A.Y., et al., *Experimental Monotonic and Cyclic Behaviour of Blind-Bolted Angle Connections.* Engineering Structures, 2009. **31**(11): p. 2540-2553.

[12] Málaga-Chuquitaype, C. and A.Y. Elghazouli, *Behaviour of Combined Channel/Angle Connections to Tubular Columns under Monotonic and Cyclic Loading.* Engineering Structures, 2010. **32**(6): p. 1600-1616.

[13] Málaga-Chuquitaype, C. and A.Y. Elghazouli, *Component-Based Mechanical Models For Blind-Bolted Angle Connections.* Engineering Structures, 2010. **32**(10): p. 3048-3067.

[14] Liu, Y., C. Málaga-Chuquitaype, and A.Y. Elghazouli, *Response and Component Characterisation of Semi-Rigid Connections to Tubular Columns under Axial Loads.* Engineering Structures, 2012. **41**(0): p. 510-532.

[15] Liu, Y., C. Málaga-Chuquitaype, and A.Y. Elghazouli, *Behaviour of Open Beam-to-Tubular Column Angle Connections under Combined Loading Conditions.* Steel and Composite Structures, 2014. **16**(2): p. 157-185.

[16] Kurobane, Y., et al., *Design Guide for Structural Hollow Section Column Connections*. 2004: TÜV-Verlag.

[17]   Mourad, E., *Behaviour of Blind Bolted Moment Connections for Square HSS Columns*, in *School of Graduated Studies*. 1993, McMaster University: Hamilton.

[18]   Park, A.Y. and Y.C. Wang, *Development of Component Stiffness Equations for Bolted Connections to RHS Columns.* Journal of Constructional Steel Research, 2012. **70**(0): p. 137-152.

[19]   Jaspart, J., et al., *Development of a Full Consistent Design Approach for Bolted and Welded Joints in Building Frames and Trusses Between Steel Members Made of Hollow and/or Open Sections– Application of the Component Method*, in *CIDECT research project 5BP, Aachen, Liege*. 2003: Aachen.

[20]   Weynand, K., J. Jaspart, and L. Ly, *Application of the Component Method to Joints between Hollow and Open Sections*, in *CIDECT research project 5BM. Aachen & Liege*. 2003, Comité International pour le Développement et l'Etude de la Construction Tubulaire: Aachen.

[21]   Thai, H.-T. and B. Uy, *Rotational stiffness and moment resistance of bolted endplate joints with hollow or CFST columns.* Journal of Constructional Steel Research, 2016. **126**: p. 139-152.

[22]   Wang, J., et al., *Seismic response investigation on CFDST column to steel beam blind-bolted connections.* Journal of Constructional Steel Research, 2019. **161**: p. 137-153.

[23]   Wang, W., et al., *Behavior and analytical investigation of assembled connection between steel beam and concrete encased CFST column.* Structures, 2020. **24**: p. 562-579.

[24]   CEN (European Committee for Standardization), *Design of steel structures - Part 1-8: Design of joints*, in *Eurocode 3: EN 1993-1-8*. 2005, CEN: Brussels, Belgium.

[25]   France, J.E., J. Buick Davison, and P. A. Kirby, *Moment-Capacity and Rotational Stiffness of Endplate Connections to Concrete-Filled Tubular Columns with Flowdrilled Connectors.* Journal of Constructional Steel Research, 1999. **50**(1): p. 35-48.

[26]   Tizani, W., M. Mahmood, and D. Bournas, *Effect of Concrete Infill and Slenderness on Column-Face Component in Anchored Blind-Bolt Connections.* Journal of Structural Engineering, 2020. **146**(4): p. 04020041.

[27]   Cao, J.J., J.A. Packer, and G.J. Yang, *Yield Line Analysis of RHS Connections with Axial Loads.* Journal of Constructional Steel Research, 1998. **48**(1): p. 1-25.

[28]   Wang, Z., Q. Wang, and W. Ouyang, *Yield Line Analysis of Bolted Connections to I-Section Webs.* Advanced Materials Research, 2010. **129**: p. 983-987.

[29]   Mahmood, M., *Column Face Bending of Anchored Blind Bolted Connections to Concrete Filled Tubular Sections*, in *Department of Civil Engineering* 2015, The University of Nottingham, UK: Nottingham.

[30]   Eligehausen, R. and J. Ozbolt. *Size Effect in Anchorage Behavior*. in *8th European Conference on Fracture Behavior and Design of Materials and Structures*. 1990. Torino, Italy: European Structural Integrity Society.

[31]   Werner Fuchs, R.E. and E.B. John, *Concrete Capacity Design (CCD) Approach for Fastening to Concrete.* Structural Journal, 1995. **92**(1): p. 73-94.

[32]   Thompson, M.K., et al., *Anchorage Behavior of Headed Reinforcement: Literature Review*. 2002, Texas Department of Transportation.

[33]   BSI, *Design of Fastenings for Use in Concrete - Part 4-2: Headed Fasteners*, in *DD CEN/TS 1992-4-1:2009*. 2009, British Standards Institution: London.